Astron. Astrophys. 292, 59–66 (1994)

ASTRONOMY AND ASTROPHYSICS

# Gaseous cocoons around compact steep spectrum sources

**F. Mantovani**[1], **W. Junor**[2], **R. Fanti**[1,3], **L. Padrielli**[1], **and D. J. Saikia**[4]

[1] Istituto di Radioastronomia del CNR, via P. Gobetti 101, I-40129, Bologna, Italy
[2] Institute for Astrophysics, University of New Mexico, Albuquerque, NM, USA
[3] Dip. di Fisica, Universitá degli Studi, Bologna, Italy
[4] Tata Institute of Fundamental Research, Pune 411 007, India

Received 13 June 1994 / Accepted 3 August 1994

**Abstract.** A small sample of five Compact Steep Spectrum Sources (CSSs) has been observed with the VLA A-array at C, X and U bands. VLA polarimetry shows that some of the sources are highly polarized with the percentage polarization ranging from 0.5% to 6%. Depolarization and very high rotation measures strongly suggest that these sources are embedded in dense gas clouds.

**Key words:** polarization – quasars: general – radio continuum: galaxies

## 1. Introduction

We began observing a small sample of steep spectrum sources at sub-arcsecond resolution several years ago. These sources were selected because there were rather clear indications (e.g. detection of low frequency variability, spectral index turnovers around 100 MHz, Fanti et al. 1983) that we were dealing with compact objects. Preliminary VLA A-array observations at $\lambda$6cm (Mantovani et al. 1992) allowed us to classify most of them as CSSs. We were able to divide those CSSs into two groups: (i) sources dominated by an unresolved steep-spectrum component and (ii) lobe-dominated sources.

The class of CSS objects has been discussed by many authors (see, for example, Pearson et al. 1985; Fanti et al. 1990). It is now accepted that CSSs are physically-small objects with sub-galactic dimensions, whose structure and sizes are probably affected by the ambient gas in the nucleus of the parent optical object. Sub-arcsecond resolution maps of CSS in quasar hosts show that these sources have strongly distorted structures with recognizable jet-like features (Fanti et al. 1986; Spencer et al. 1991), consistent with strong dynamical interactions between jets and the ambient media.

Most CSSs show low percentage polarizations ($\sim 1\%$) at or below 5 GHz (Saikia 1991) though there are notable exceptions like 3C138 and 3C286. To explain both their low polarizations at centimeter wavelengths and small sizes, it has been postulated that CSSs are cocooned in dense gaseous envelopes. The polarization properties of CSSs at frequencies above 5 GHz have been little investigated. Consequently, it is not known whether the low observed polarizations of CSSs below 10 GHz are due mostly to large RMs arising within the sources and their host objects.

The results of our investigations at sub-arcsecond resolutions for the five sources in our sample of CSSs which showed large Faraday Rotation Measures (RMs) are presented here.

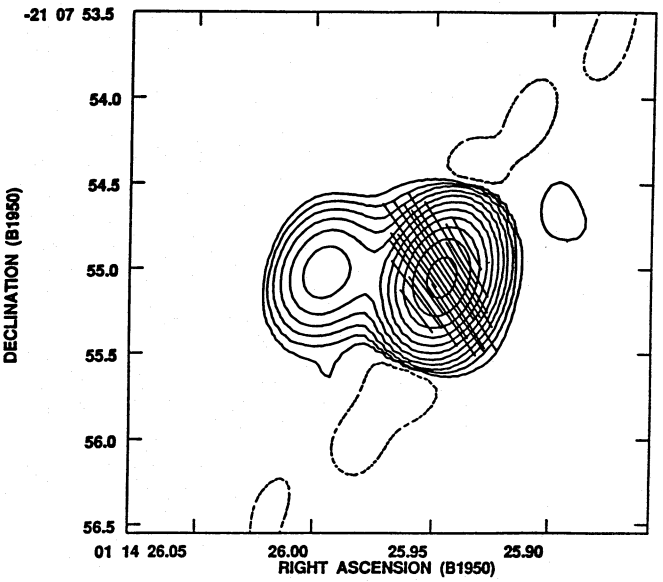


**Fig. 1.** VLA image of 0114−211 at 8.4 GHz. Contours are at −0.5, 0.5, 1, 2, 4, 8, 16, 32, 64, 128, 256, 512 mJy beam$^{-1}$. The peak flux density is 680.0 mJy beam$^{-1}$. A vector length of 1″ = 20 mJy beam$^{-1}$

## 2. VLA observations

VLA (Thompson et al. 1980) A-array observations were made in the C (5 GHz) band (May 30th, 1986), and X (8.4 GHz)

*Send offprint requests to*: F. Mantovani

**Table 1.** Observational parameters and observed properties

| Source | Obs. $\nu$ MHz | Beam maj. $''$ | Beam min. $''$ | PA $^\circ$ | $\sigma_t$ mJy/b | $\sigma_p$ mJy/b | C | R.A.(B1950) h m s | Dec.(B1950) $^\circ$ $'$ $''$ | Flux peak mJy/b | Dens. total mJy |
|---|---|---|---|---|---|---|---|---|---|---|---|
| 0114−211 | 4885 | 0.43 | 0.37 | 36 | 0.18 | 0.20 | a+b | 01 14 26.00 | −21 07 54.97 | 61 | 71 |
| | | | | | | | c | 25.95 | 55.00 | 1071 | 1105 |
| | 8440 | 0.39 | 0.27 | −18 | 0.05 | 0.06 | a+b | 25.99 | 55.02 | 23.8 | 31.9 |
| | | | | | | | c | 25.95 | 55.05 | 698.5 | 728.6 |
| | 14940 | 0.23 | 0.15 | −4 | 0.13 | 0.20 | a | 26.00 | 54.98 | 5.2 | 6.0 |
| | | | | | | | b | 25.98 | 54.98 | 2.8 | 3.2 |
| | | | | | | | c | 25.95 | 55.00 | 358.9 | 371.9 |
| 0548−165 | 4885 | 0.35 | 0.34 | −36 | 0.06 | 0.14 | a | 05 48 25.20 | 16 35 56.80 | 892 | 938 |
| | | | | | | | b | 25.16 | 59.59 | 8 | 24 |
| | 8440 | 0.29 | 0.22 | 59 | 0.07 | 0.07 | a | 25.20 | 56.97 | 589.9 | 633 |
| | | | | | | | b | 25.16 | 59.83 | 3.1 | 5.4 |
| | 14940 | 0.18 | 0.13 | 68 | 0.12 | 0.16 | a | 25.20 | 56.98 | 288.7 | 310.2 |
| 0725+147 | 4885 | 0.34 | 0.33 | 87 | 0.10 | 0.10 | a | 07 25 20.49 | 14 43 44.60 | 321 | 439 |
| | | | | | | | b | 20.22 | 46.54 | 9 | 9 |
| | | | | | | | c | 20.11 | 47.17 | 131 | 227 |
| | 8440 | 0.24 | 0.21 | 35 | 0.02 | 0.03 | a | 20.49 | 45.95 | 198.9 | 281.3 |
| | | | | | | | b | 20.21 | 46.89 | 6.3 | 6.3 |
| | | | | | | | c | 20.11 | 47.52 | 52.7 | 106.2 |
| | 14490 | 0.13 | 0.12 | 37 | 0.07 | 0.11 | a | 20.48 | 44.92 | 91.5 | 141.8 |
| | | | | | | | b | 20.22 | 46.86 | 3.7 | 3.9 |
| | | | | | | | c | 20.11 | 47.50 | 12.3 | 35.2 |
| 1245−197 | 4885 | 0.47 | 0.36 | −29 | 0.10 | 0.30 | a | 12 45 45.22 | −19 42 57.51 | 2296 | 2388 |
| | 8440 | 0.30 | 0.21 | 25 | 0.06 | 0.06 | a | 45.21 | 57.44 | 1355 | 1623 |
| | 14490 | 0.17 | 0.12 | 26 | 0.10 | 0.15 | a | 45.22 | 57.49 | 930.1 | 980.1 |
| 1524−136 | 4885 | 0.39 | 0.38 | −44 | 0.08 | 0.10 | a+b | 15 24 12.89 | −13 40 34.93 | 924 | 1184 |
| | 8440 | 0.27 | 0.23 | 31 | 0.06 | 0.05 | a+b | 12.87 | 34.95 | 685.4 | 723.0 |
| | 14490 | 0.15 | 0.13 | 30 | 0.10 | 0.21 | a | 12.86 | 35.15 | 63.0 | 82.0 |
| | | | | | | | b | 12.87 | 34.90 | 406.0 | 515.0 |

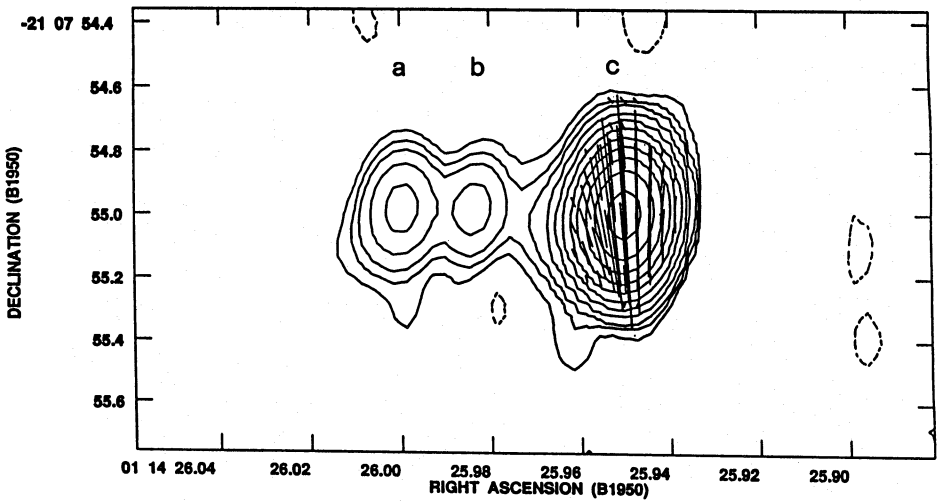


**Fig. 2.** VLA image of 0114−211 at 15 GHz. Contours are at −0.3, 0.3, 0.6, 1, 2, 4, 8, 16, 32, 64, 128, 256, 512 mJy beam$^{-1}$. The peak flux density is 358.9 mJy beam$^{-1}$. A vector length of 1$''$= 25 mJy beam$^{-1}$

**Table 2.** Polarization parameters

| Source | $z$ | C | PA | | | RM | RM× | %Pol | | | DP | DP |
|---|---|---|---|---|---|---|---|---|---|---|---|---|
| | | | 6cm | 4cm | 2cm | | $(1+z)^2$ | 6cm | 4cm | 2cm | 6-4 | 4-2 |
| 0114−211 | (0.5) | c | 140±10 | 36± 2 | 4± 2 | 646 | 1450 | 1.6 | 3.3 | 5.0 | 0.48 | 0.66 |
| 0548+165[a] | 0.474 | a | 264± 4 | 120± 2 | 92± 1 | 890 | 1934 | 1.5 | 2.9 | 3.6 | 0.52 | 0.80 |
| 0725+147 | 1.382 | a | 80± 1 | 69± 5 | 63± 3 | 96 | 545 | 6.3 | 6.2 | 6.1 | ∼1 | ∼1 |
| | | c | 85± 2 | 148± 3 | 164± 2 | −454 | −2576 | 0.5 | 2.7 | 6.0 | 0.19 | 0.45 |
| 1245−197 | 1.275 | a | 246± 7 | 113± 5 | 76± 3 | 942 | 4875 | 0.5 | 0.3 | 0.4 | ∼1 | ∼1 |
| 1524−136 | 1.687 | b | 62± 5 | 85± 2 | 86± 2 | −116 | −840 | 2.7 | 2.5 | 2.7 | ∼1 | ∼1 |

[a] redshift from Lipovetskii et al. 1989.

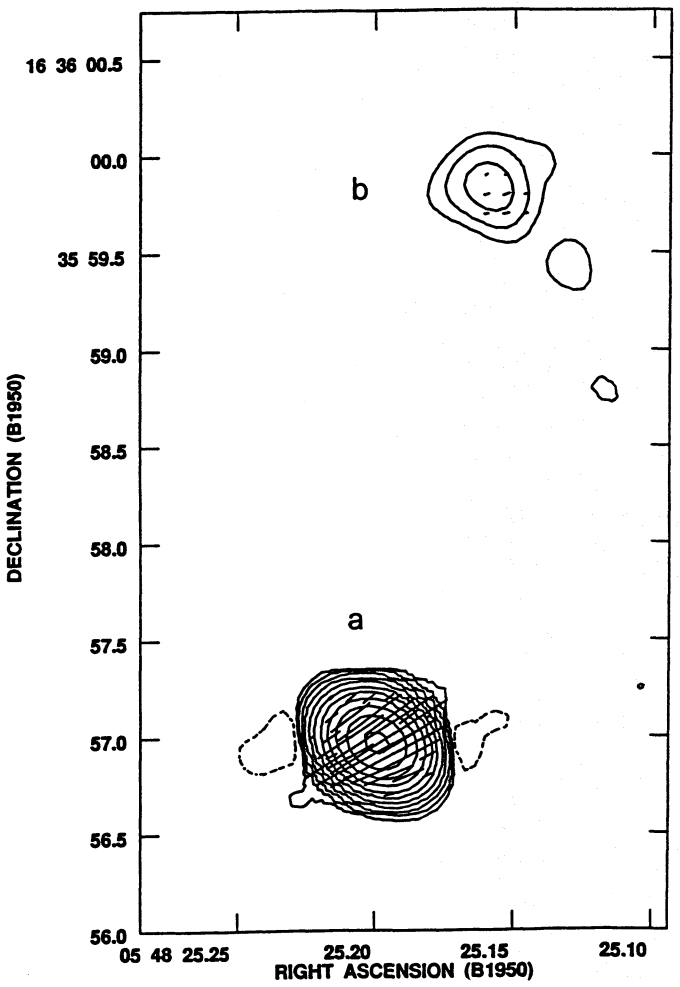


**Fig. 3.** VLA image of 0548+165 at 8.4 GHz. Contours are at −0.5, 0.5, 1, 2, 4, 8, 16, 32, 64, 128, 256, 512 mJy beam$^{-1}$. The peak flux density is 589.9 mJy beam$^{-1}$. A vector length of 1″= 20 mJy beam$^{-1}$

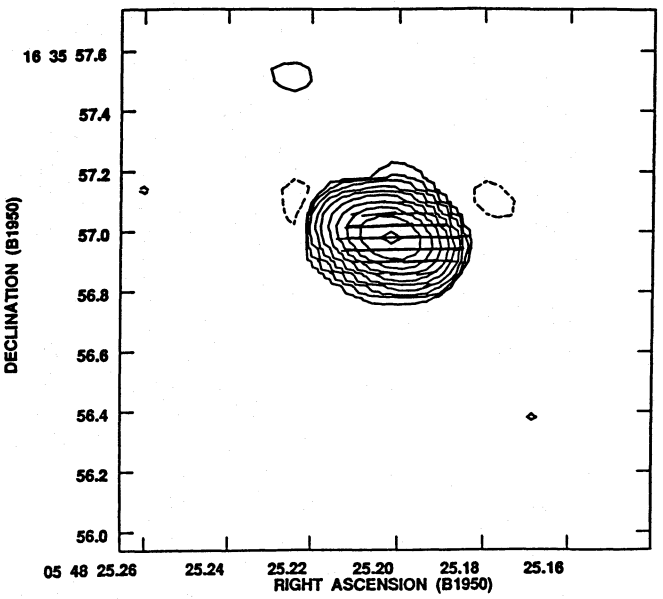


**Fig. 4.** VLA image of 0548+165 at 15 GHz. Contours are at −0.5, 0.5, 1, 2, 4, 8, 16, 32, 64, 128, 256, 512 mJy beam$^{-1}$. The peak flux density is 288.7 mJy beam$^{-1}$. A vector length of 1″= 25.0 mJy beam$^{-1}$

and U (15 GHz) bands (September 10th, 1990). The data were calibrated in the standard way using VLA calibrators and AIPS procedures. The VLA receivers are sensitive to Left-hand (L) or Right-hand (R) circularly polarized radiation. An iterative procedure was carried out using the MX and CALIB programs to self-calibrate the parallel-hand (LL or RR) fringes. The complex gain corrections so derived were also applied to the cross-hand (RL or LR) fringes. In turn, images in Stokes parameters I, Q, and U were produced. Maps of the polarized flux density $P = (Q^2 + U^2)^{1/2}$ and position angle $\chi = 0.5 \times tan^{-1}(U/Q)$, were then generated from the Q and U images.

## 3. VLA structure and polarimetry of CSSs

### *3.1. Observational parameters*

The Total Intensity images at 5 GHz for the sources listed in Table 1 were presented in Mantovani et al. (1992). However, observational parameters and observed properties obtained from the VLA observations at 5 GHz are incorporated in Table 1 to aid the reader. Maps at higher resolution have been obtained at 8.4 and 15 GHz with the VLA in the A configuration. Values derived from the maps are listed in Table 1. The contents of Table 1 are: column 1 – source name; column 2 – the observing frequency in MHz; columns 3 to 5 – major axis, minor axis (both in arcsec)

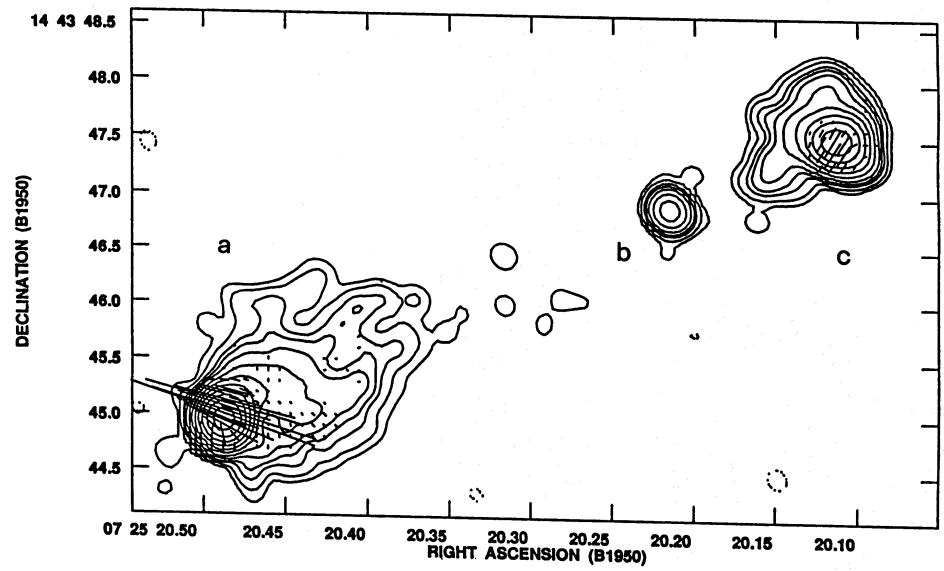


**Fig. 5.** VLA image of 0725+147 at 8.4 GHz. Contours are at −0.1, 0.1, 0.2, 0.4, 0.6, 1, 2, 4, 8, 16, 32, 64, 128, 256, 512 mJy beam$^{-1}$. The peak flux density is 201.4 mJy beam$^{-1}$. A vector length of 1″= 8.0 mJy beam$^{-1}$

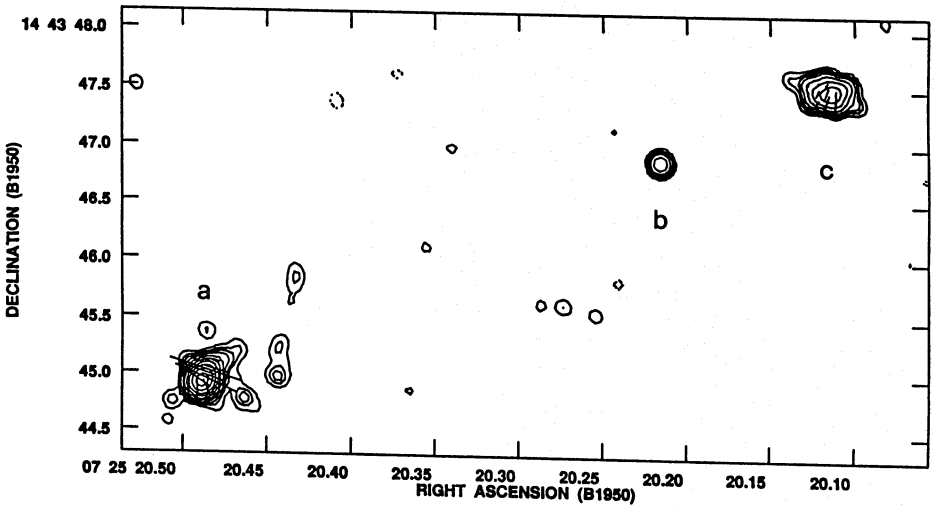


**Fig. 6.** VLA image of 0725+147 at 15 GHz. Contours are at −0.2, 0.2, 0.4, 0.6, 1, 2, 4, 8, 16, 32, 64, 128, 256, 512 mJy beam$^{-1}$. The peak flux density is 91.5 mJy beam$^{-1}$. A vector length of 1″= 10.0 mJy beam$^{-1}$

and the PA in degrees of the restoring beam major axis; column 6 – the rms noise in the total intensity map far from the source of emission; column 7 – the rms noise $\sqrt{\sigma_Q^2 + \sigma_U^2}$, where $\sigma_Q$ and $\sigma_U$ are the rms noise on the blank sky in the distributions of the Stokes parameters Q and U; column 8 – component label; columns 9 and 10– RA and Dec. of the component peak; column 11 – peak flux density (mJy) of the component; column 12 – total flux density (mJy) of the component.

### *3.2. Notes on individual sources*

#### 3.2.1. 0114–211

The 15 GHz VLA image has enough resolution to show that a weaker component exists between the two components already seen at lower frequencies. The *c* component (which is the brightest) is strongly polarized at the three observing frequencies. Polarization was not detected from the two weaker components. There are some indications on the smoothed 15 GHz map of polarized emission at the outer edge of component *a*. This, and a recent (Mantovani et al. 1994) VLBI image at $\lambda$18cm of 0114–211 which shows a triple structure which agrees quite well with the VLA image, suggests that the central component, *b*, is the core. The images at 8.4 GHz and 15 GHz are presented in Figs. 1 and 2 respectively.

#### 3.2.2. 0548+165

The existence of the component North of the main one is confirmed by the 8.4 GHz image (Fig. 3) but it is not detected at 15 GHz (Fig. 4). The emission from this faint extended component is also weakly polarized at 8.4 GHz. Most of the polarized flux density comes from the main component, however.

#### 3.2.3. 0725+147 (3C181)

This has been classified as a lobe-dominated CSS. The X band image is quite similar to the 5 GHz one. At 15 GHz the central component is still visible. The extended emission in both lobes has almost disappeared. Only the bright hot spots are visible

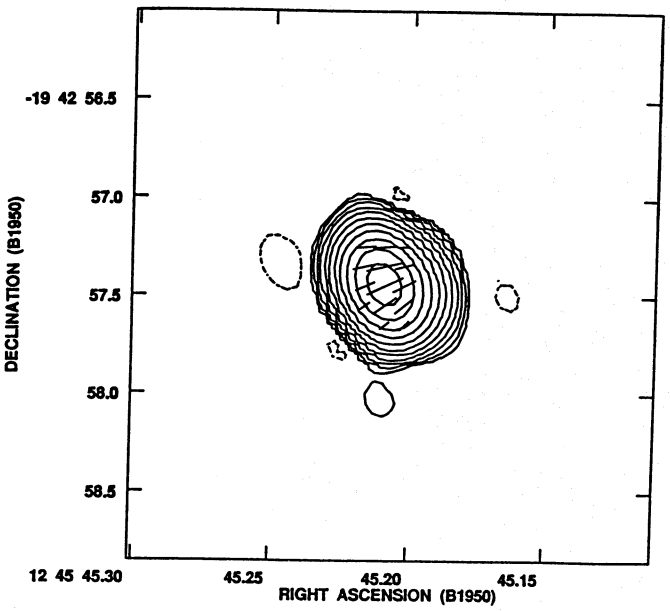


**Fig. 7.** VLA image of 12455−197 at 8.4 GHz. Contours are at −1, 1, 2, 4, 8, 16, 32, 64, 128, 256, 512 mJy beam$^{-1}$. The peak flux density is 1552.6 mJy beam$^{-1}$. A vector length of 1″= 6.7 mJy beam$^{-1}$

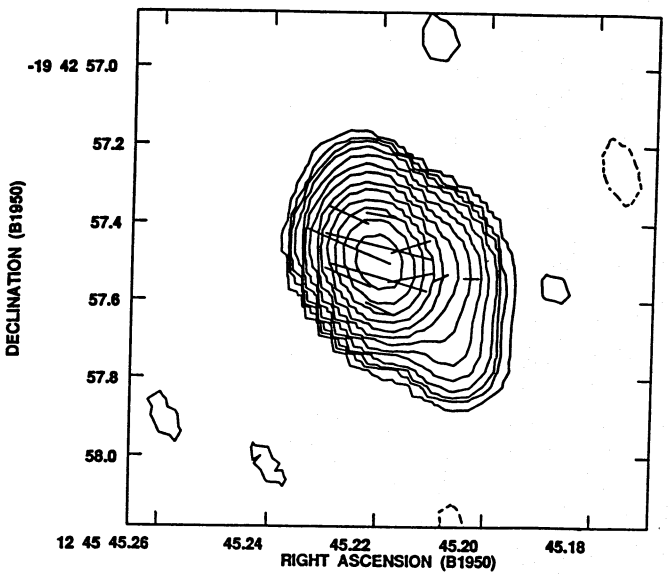


**Fig. 8.** VLA image of 1245−197 at 15 GHz. Contours are at −0.2, 0.2, 0.4, 0.6, 1, 2, 4, 8, 16, 32, 64, 128, 256, 512 mJy beam$^{-1}$. The peak flux density is 930.7 mJy beam$^{-1}$. A vector length of 1″= 8.3 mJy beam$^{-1}$

there. Most of the polarized emission comes from these regions. The lobe around the hot spot labelled *a* is weakly polarized down to 5 GHz. Hot spot *c* is less polarized than *a* and the diffuse emission around it is not polarized. No polarization was detected in the central component. The images at 8.4 GHz and 15 GHz are shown in Figs. 5 and 6 respectively.

#### 3.2.4. 1245−197

The source structure at 8.4 GHz is extended slightly in the south-west direction (Fig. 7). This is more evident in the 15 GHz image (Fig. 8). Most of the polarized emission comes from the central unresolved region.

#### 3.2.5. 1524−136

The source 1524−136 has a double structure which is visible at 15 GHz. The ratio between the two peaks of emission is ∼13. The weaker component has a percentage polarized flux which is almost a factor two larger than the other. Figures 9 and 10 show the images at 8.4 GHz and 15 GHz respectively.

### *3.3. VLA polarimetry*

The images obtained at 8.4 GHz and 15 GHz were convolved with a two-dimensional, circularly-symmetric Gaussian with a width of ∼0.4 arcsec. This approximates the resolution of the synthesized beam of the VLA A-array at 5 GHz. Observational parameters were calculated from the new images. These are summarized in Table 2 as follows: column 1 − source name; column 2 − the measured redshift. (Where redshift information was not available a value of $z = 0.5$ was assumed.); column 3 − component label; columns 4 to 6 − PA in degrees of the electric field vector at the peak of polarized emission (±1 rms error calculated from the distribution of PAs found in a small box around the peak of polarized emission) at 5, 8.4 and 15 GHz respectively; column 7 − the Rotation Measure (RM=d$\phi(\lambda)$/d($\lambda^2$) in rad m$^{-2}$, where $\phi(\lambda)$ is the PA at wavelength $\lambda$ computed by fitting the points plotted in Fig. 11 with a least-squares linear fit (see below); column 8 − the RM corrected for the redshift; columns 9 to 11 − polarization percentage at 5, 8.4 and 15 GHz respectively; columns 12 and 13 − the depolarization index, defined as the ratio of the fractional polarization at longer wavelength and the fractional polarization at shorter wavelength.

## 4. Discussion

In Fig. 11a–f plots of the PA versus $\lambda^2$ are given for the five sources. The error bars are $\pm 1 \times rms$. All of the sources follow $\lambda^2$ laws reasonably well — with the exception of 0548+165 for which the fit is questionable. Extrapolation of the fitted rotation law to $\lambda \Rightarrow 0$ gives the intrinsic value of the PA of the electric vector. For all of the sources, except 1245−197, the E vector is perpendicular to the source major axis. This is commonly the case for VLBI-scale jets in quasars (see, for example, Roberts et al. 1989). The RM values we have obtained (listed in column 8 of Table 2) are large. We can compare them with those in the compilation by Taylor et al. (1992) of extragalactic radio sources known to have RMs> 700 rad m$^{-2}$. Of those, seven out of fifteen sources are CSSs. The result of an investigation by K. Aizu is reported in that paper. He found that, out of ten sources known to have RMs in excess of 1000 rad m$^{-2}$, seven are CSSs. Therefore, it is not surprising that we find in our small sample of CSSs with detectable polarization that a large fraction of them

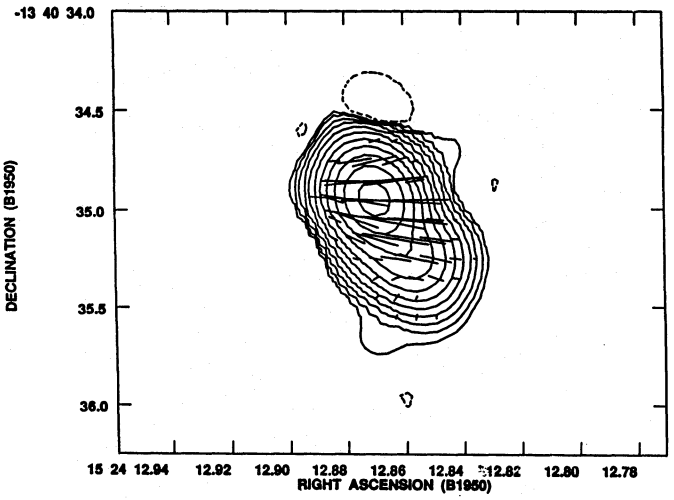


**Fig. 9.** VLA image of 1524−136 at 8.4 GHz. Contours are at −0.5, 0.5, 1, 2, 4, 8, 16, 32, 64, 128, 256, 512, 1024 mJy beam$^{-1}$. The peak flux density is 685.4 mJy beam$^{-1}$. A vector length of 1″= 20.0 mJy beam$^{-1}$

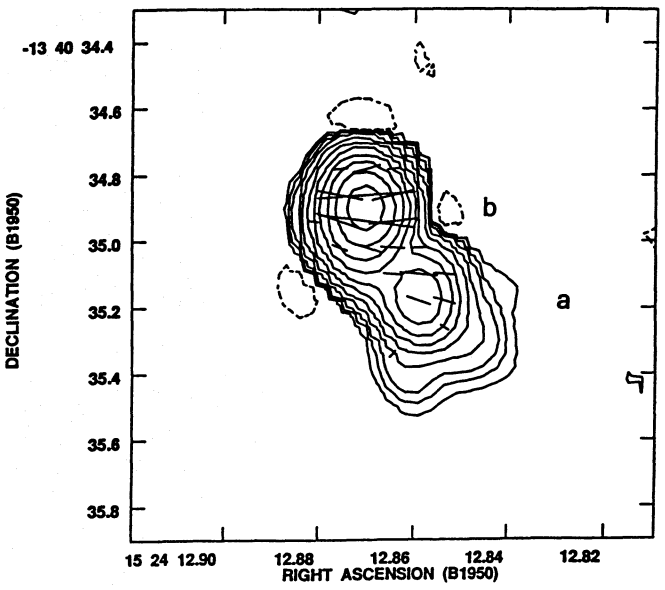


**Fig. 10.** VLA image of 1524−136 at 15 GHz. Contours are at −0.3, 0.3, 0.6, 1, 2, 4, 8, 16, 32, 64, 128, 256, 512, 1024 mJy beam$^{-1}$. The peak flux density is 406.4 mJy beam$^{-1}$. A vector length of 1″= 25.0 mJy beam$^{-1}$

show very high RMs. In Table 2 we also report the values for the percentage polarization at each frequency and the depolarization ratio DP. About half of the cases show decreasing percentage polarization going from higher to lower frequencies, namely the sources 0114−211, 0548+165 and component *c* of 0725+145. The remaining sources (1245−197, 1524−136 and component *a* of 0725+145) show no depolarization between 15 GHz and 5 GHz. Such a trend persists at frequencies below 5 GHz for those sources for which total power measurements are available, i.e. all but 0114−211 (see Tabara & Inoue 1980).

There appear to be two physical situations: (1) a $\lambda^2$ rotation law with no depolarization, which indicates the presence of a screen between the source of emission and the observer (as in 1245−197 and 1524−136), and (2) a $\lambda^2$ rotation law (with observed rotation $< \pi/2$) and depolarization (0114−211 and 0548+165), which suggests co-extensive synchrotron-emitting regions and thermal plasma (see, for example, Burn 1966). In this case, however, the $\lambda^2$ law would not be followed at longer wavelengths.

Particularly interesting is the case of the lobe-dominated source 0725+147, in which both physical conditions occur. 0725+147 has one lobe with RM= 545 rad m$^{-2}$ and constant fractional polarization. The other lobe has RM= −2576 rad m$^{-2}$ and strong depolarization. Single baseline polarization observations of 0725+145 at $\lambda\lambda$18, 31cm have been made with a 23.7 km-long, radio-linked interferometer (Davis et al. 1983). The PAs measured at the two wavelengths, corrected by $n\pi$, are plotted in Fig. 11d, together with the values from this paper. This plot shows that the $\lambda^2$ law continues over a wide range of frequencies for both lobes. Moreover, the percentage of polarization is constant down to $\lambda$18cm for lobe *a* and decreases to 2.4% at $\lambda$31cm. The trend of decreasing fractional polarization in lobe *c* is confirmed by the Davis et al. measurements.

Such asymmetric depolarization is often observed in the lobes of FRII extended galaxies. Following Garrington & Conway (1991), it appears that component *a* in 0725+147 is closer to us and the observed emission traverses a shorter path length through the depolarizing medium in and/or around the lobe. Receding component *c* shows depolarization and follows a $\lambda^2$ law over a wide range of frequencies (down to at least 962 MHz) which suggests that the line-of-sight to this lobe travels a longer path length through the thermal medium.

Of course, these observations are unable to discern the actual location of the depolarizing medium. This medium may be either co-extensive with a synchrotron-emitting region or may lie outside these regions and envelope the source.

## 5. Conclusions

Our results are of great importance for the understanding of the physics of CSSs. The number of sources in the present investigation from which we have extracted these five sources is rather small and this, along with the selection criteria, precludes statistical investigation. However, we can reach the following conclusions:

1. The sources show a notable degree of polarized emission, ranging from 0.5% to 6%.
2. In all cases the polarization position angle follows a $\lambda^2$ law. This strongly indicates that there are gaseous cocoons around these sources.
3. The de-rotated magnetic fields are parallel to the source major axis.
4. About half of these sources have $\lambda^2$ rotation laws with depolarization. In these cases we cannot exclude the possi-

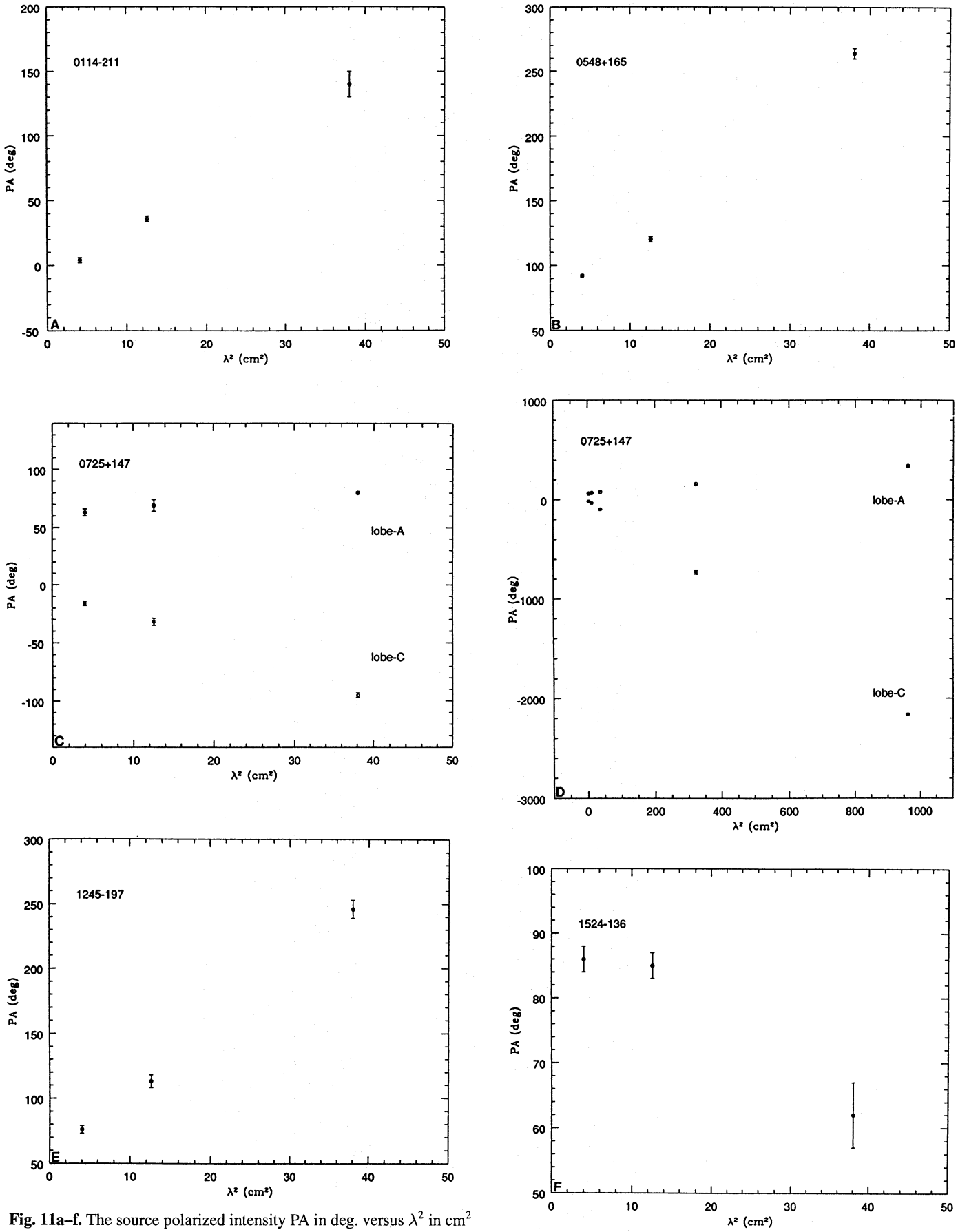


**Fig. 11a–f.** The source polarized intensity PA in deg. versus $\lambda^2$ in $cm^2$

bility that the RM may also occur in the emitting region itself. The angular resolution of these observations is insufficient to decide if thermal material is coextensive with the synchrotron-emitting plasma. VLBI polarimetry is required to discriminate between the possibilities.

5. 0725−147 has a polarization asymmetry that can be explained with a Garrington & Conway (1991) type of model.

These observations support the view that CSSs are objects where unusual conditions of the interstellar medium inhibit the radio source from growing to larger dimensions, more typical of normal extragalactic radio sources.

*Acknowledgements.* The authors wish to thank the referee, Prof. R.G. Conway, for his suggestions. FM thanks Miller Goss, Assistant Director, NRAO, Socorro, for his hospitality during period when part of the work was done. The National Radio Astronomy Observatory is operated by Associated Universities Inc., under cooperative agreement with the National Science Foundation; AIPS is NRAO's *Astronomical Image Processing System*.

## References

Burn, B. J. 1966, MNRAS 133, 67

Cotton, W. D., Owen, F. N., Geldzahler, B. J., Johnston, K., Bååth, L., Romney, J. 1984, ApJ 277, L41

Davis, R. J., Stannard, D. and Conway, R, G., 1983, MNRAS 205, 1267

Fanti, C., Fanti, R., Schilizzi, R. T., Spencer, R. E., van Breugel W. J. M. 1986, A&A 170, 10

Fanti, R., Fanti, C., Schilizzi, R. T., Spencer, R. E., Rendong Nan, van Breugel W. J. M. and Venturi, T. 1990, A&A 231, 333

Garrington, S.T. and Conway, R.G. 1991, MNRAS 250, 198

Mantovani, F., Saikia, D.J., Browne, I.W.A., et al., 1990, MNRAS 245, 427

Mantovani, F., Junor, W., Fanti, R., et al., 1992, MNRAS 257, 353

Mantovani, F., Junor, W. and Bondi, M. 1994, Compact Extragalactic Radio Sources, Proceedings of a Workshop held in Socorro, New Mexico, Feb. 11-12, 1994, ed. J.A. Zensus and K.I. Kellermann, pag. 29

Muxlow, T. W. B. 1993, in Sub-arcsecond Radio Astronomy, ed. R. J. Davis and R. S. Booth (Cambridge: Cambridge University Press), pag. 252.

Pearson, T. J., Perley, R. A., Readhead, A. C. S. 1985, AJ 90, 738

Roberts, D.H, Wardle, J.F.C., Brown, L.F., Gabuzda, D.C. and Cawthorne, T.V. 1989, Parsec-Scale Radio Jet, ed. J.A. Zensus and T.J. Pearson (Cambridge: Cambridge University Press), 110.

Saikia, D. J. 1991, Compact Steep-Spectrum and GHz-Peaked Spectrum Radio Sources, ed. C. Fanti, R. Fanti, C. P. O'Dea and R. T. Schilizzi (Bologna: C.N.R. Istituto di Radioastronomia), p. 12

Spencer, R. E., Schilizzi, R. T., Fanti, C., et al., 1991, MNRAS 250, 225

Tabara, H., Inoue, M. 1980, A&AS 39, 379

Taylor, G. B., Inoue, M., Tabara, H. 1992, A&A 264, 421

Thompson, A. R., Clark, B. G., Wade, C. M., Napier, P.J. 1980, ApJS 44, 151

This article was processed by the author using Springer-Verlag LaTeX A&A style file *L-AA* version 3.